Third-Body Stabilization of Supercritical CO₂ in CO Oxidation: Development and Application of a New ReaxFF Force Field for the CO/O/CO₂ System

Emdadul Haque Chowdhury¹, Masoud Aryanpour², Yun Kyung Shin¹, Bladimir Ramos-Alvarado¹, Matthias Ihme³, Adri van Duin^{1,a)}

¹Department of Mechanical Engineering, The Pennsylvania State University, University Park, PA16802, USA.

²Independent Researcher

³Department of Mechanical Engineering, Stanford University, Stanford CA 94305, USA

a) Corresponding author: acv13@psu.edu

Abstract

Supercritical CO₂ (scCO₂) plays a crucial role as a solvent in separation processes, advanced power cycles, and "green" chemical and materials processing. Nonetheless, the atomistic comprehension of how the dense scCO₂ matrix influences the fundamental combustion of carbon monoxide (CO) is still insufficiently explored. Experimental studies and traditional molecular dynamics (MD) simulations frequently fail to detect the highly reactive, transient intermediates, such as atomic oxygen (O), that drive these reactions. To fill this knowledge gap, we have developed a novel ReaxFF reactive force field for the CO₂/CO/O system. To effectively model CO₂ crystal properties, intermolecular interactions, bond energies, and critical reaction energy barriers, the force field parameters were calibrated using data obtained from the density functional theory and secondorder Møller-Plesset calculations. The force field was able to reproduce the cohesive energy of the CO₂ crystal, the pressure characteristics of bulk scCO₂, and the structural properties of liquid and scCO₂, as documented by experiments, ab-initio MD, and prominent non-reactive models. The force field was subsequently applied to study the $CO + O \rightarrow CO_2$ reaction. In a dilute gas-phase environment, the reaction exhibits inefficiency as the newly formed CO₂ rapidly dissociates back due to substantial kinetic energy acquired from the exothermic reaction. Conversely, in a dense scCO₂ environment, the surrounding CO₂ matrix acts as an efficient third body, stabilizing the emerging CO₂ product by dissipating its excess energy via molecular collisions. As such, this ReaxFF force field facilitates a unique, large-scale reactive MD description of radical chemistry in scCO₂ and establishes a mechanistic foundation for third-body stabilization in dense reactive environments.

1. Introduction

High-pressure supercritical fluid (SCF) technologies are becoming more inventive and sustainable in modern industry. A fluid is classified as supercritical when it is maintained at a temperature and pressure above its critical point, leading to a unique set of physical properties. A substance in this state exhibits liquid-like density and solvating capacity, while maintaining gas-like low viscosity and high diffusivity.

Among these, supercritical carbon dioxide (scCO₂) is the most widely utilized SCF due to the combination of some highly advantageous properties.^{3,4} Its mild critical conditions (31.1°C and 73.8 bar) makes it attractive for thermally sensitive materials processing.^{5,6} In addition, its non-flammability, non-toxicity, and abundance in high purity earn it a "generally recognized as safe" (GRAS) status². Compared to conventional solvents, it exhibits superior mass transfer and penetration capabilities owing to its low viscosity, high diffusivity, and negligible surface tension.^{7,8} Furthermore, its solvent properties can be tuned by temperature and pressure variation, which can alter the reaction kinetics, making it an appealing reaction medium.⁹ This render it a promising candidate for carbon capture and storage (CCS).¹⁰ In addition, its contribution in the energy sector is becoming increasingly important. The advantageous thermophysical properties render it a suitable working fluid for advanced power cycles, facilitating enhanced thermal efficiency and more compact turbomachinery.^{5,9} Quantum mechanical (QM) studies indicate that scCO₂ functions not only as an inert diluent but also actively influences combustion by stabilizing reactive intermediates and providing alternative reaction pathways.¹¹

Understanding carbon monoxide (CO) chemistry is important for optimizing the operation of scCO₂-based combustion systems. CO is an important pollutant and intermediate, and its accumulation poses both environmental and health hazards. ^{12,13} In direct-fired scCO₂ power cycles and other advanced combustion systems, complete CO oxidation is crucial for operational stability and efficiency. ¹⁴ Experiments and kinetic analyses demonstrated that the primary reaction for CO oxidation in hydrocarbon flames is: CO + OH \rightleftharpoons CO₂ + H; and the conversion of CO via CO + O₂ \rightarrow CO₂ + O is slow and insignificant in the presence of a large concentration of radical (OH, H, O, HO₂) pool. ^{15–17} In strongly backmixed CO-air systems and in high-temperature oxy-fuel or

scCO₂ flames, atomic O can persist at super-equilibrium level, contributing directly to CO oxidation and indirectly to OH regenerating through O + $H_2O \rightarrow 2OH$ and O + $H_2 \rightarrow OH$. ^{14,18–21} As such, a comprehensive understanding of how O radicals govern CO oxidation in scCO₂ flames is indispensable for accurate kinetic modeling.

Numerous experimental studies have been conducted to elucidate the kinetics of CO combustion. 21-23 While such investigations yielded significant insights into macroscopic observables (rates, ignition delays, flame speed, burnout times), they failed to illuminate the intricate radical chemistry underneath. 12,16,24 The high reactivity and brief lifespan of O radicals and other intermediates, such as CO₃, pose significant challenges for experiments to determine their precise collision dynamics, particularly under high pressure and in scCO₂. These constraints necessitate the utilization of computational methods to interpret the experimental observations and disclose the intricate reaction mechanisms. Researchers extensively leveraged molecular dynamics (MD) simulations to investigate the atomistic details of scCO₂ and combustion systems.^{25–31} Primarily, those studies employed classical, non-reactive force fields and ab-initio MD to examine the thermodynamic and structural characteristics of scCO₂, including solubility, induced dipole effects, phase behavior and its mixtures with co-solvents. 25-27,32 The investigations on the impact of scCO₂ on ignition delay and combustion characteristics demonstrated that CO₂ dilution modifies flame dynamics in CH₄ systems.³³ These force fields are useful for understanding physical behavior, but they rely on predetermined atomic connectivity and cannot capture dynamic bond formation and dissociation events.¹⁰ Ab-initio simulations, on the other hand, are too computationally costly to study solvent-mediated radical stabilization, which requires large system sizes and time scales.¹⁰

The ReaxFF reactive force field was developed to bridge this critical gap. ^{34–36} By employing a bond-order-based framework, it can track continuous formation and breaking of chemical bonds, rendering it an effective tool to investigate complex chemical reactions. ReaxFF parameters are trained extensively on QM data, allowing it to achieve accuracy comparable to QM methods with a substantially reduced computing cost. This capability allows ReaxFF to simulate thousands of atoms over nanoseconds, making it effective for investigating chemical reactions in a bulk supercritical environment. ^{37–40} ReaxFF has been effectively applied to a range of combustion phenomena, including the pyrolysis and high-temperature oxidation of hydrocarbons

such as methane and propene,⁴¹ the oxidation of methanol in supercritical environments,³³ the oxyfuel combustion and pyrolysis of coals,^{42,43} syngas combustion,⁴⁴ and oxidation of iron surfaces in scCO₂.⁴⁵ For example, oxy-fuel coal combustion in O₂/CO₂ environments elucidated CO₂ formation mechanisms and demonstrated that elevated CO₂ concentrations enhance reaction rates while lowering O₂ consumption.⁴⁶ In addition, oxy-combustion of syngas in scCO₂ demonstrated modified ignition chemistry and underscored the catalytic functions of CO₂.^{33,44,47}

Furthermore, ReaxFF simulations reveal that solvents do not always serve as inert environments, but can play a crucial role in stabilizing highly energetic intermediates and products via collisional energy transfer and solvent cage effects, e.g., ReaxFF simulations of methanol oxycombustion in supercritical H₂O (scH₂O) environment indicate that scH₂O acts as an effective third body to dissipate excess energy and promote stable product formation, and significantly accelerates methanol decomposition.³³ Another ReaxFF study of Fe oxidation in scCO₂ demonstrated temperature-dependent direct participation of scCO₂ in surface reactions.⁴⁵ At 600 K, scCO₂ adsorbs on the iron surface, forming a passivating FeCO₃ layer. At 1000 K, however, scCO₂ decomposes into CO, O, and C adatoms, resulting in FeO and Fe₃C formation. A recent ReaxFF study indicated that supercritical xenon facilitates iodine recombination by transferring excess energy. 48 These examples underscore the ability of supercritical solvents in product stabilization and their active involvement in reaction chemistry. Likewise, the dense scCO2 matrix may significantly aid in stabilizing the nascent high-energy CO₂ molecule produced from the exothermic reaction of CO and O. Despite its significance, a ReaxFF analysis elucidating the atomistic aspects of the CO + O → CO₂ reaction and the influence of bulk scCO₂ environment on stable product formation has not been adequately explored. To address the current knowledge gap, this article introduces a novel ReaxFF reactive force field developed for the CO/O/CO2 system. This force field is employed to predict physical properties of CO₂, including the equation of state and cohesive energy, as well as to simulate the reaction dynamics of CO + O in both a dilute and a dense scCO₂ environment. This comparative analysis aims to clarify the role of the scCO₂ solvent as a third body in stabilizing highly exothermic reaction products.

2. Methodology

2.1 ReaxFF Force Field

ReaxFF is a bond order-based force field that can accurately represent bond formation and breaking events across various materials and chemical systems.^{36,41} ReaxFF dynamically assesses connectivity via bond orders derived from updated interatomic distances at each MD iterations, whereas traditional nonreactive force fields depend on fixed, predefined connectivity. ReaxFF is typically parameterized mainly against quantum mechanical (QM) reference data, enabling it to attain near-QM accuracy while functioning at a significantly faster computational speed. This efficiency facilitates the simulation of large systems across prolonged time scales. Moreover, nonreactive force fields typically employ fixed atomic charges that remain constant throughout the MD simulations, but ReaxFF incorporates a polarizable charge equilibration method (EEM or ACKS2)⁴⁹ that recalculates atomic charges at each iteration based on the local chemical environment. ReaxFF determines the total system energy that governs atomic forces using the following equation:

$$E_{sys} = E_{bond} + E_{over} + E_{under} + E_{lp} + E_{val} + E_{tor} + E_{vdWaals}$$

$$+ E_{coulomb}$$
(1)

This total system energy (E_{sys}) accounts for bond formation and dissociation (E_{bond}) , over/under coordination penalties (E_{over}/E_{under}) , lone-pair energy (E_{lp}) , valence angle strain (E_{val}) , and dihedral angle strain (E_{tor}) , as well as non-bonded van der Waals $(E_{vdWaals})$ and electrostatic interactions $(E_{coulomb})$. For a more detailed description of the ReaxFF potential functions, readers are referred to the supporting information of Chenoweth et al.⁴¹

2.2 Force Field Parameter Training

The ReaxFF force field is system-dependent and necessitates parameter optimization for precise representation. The parameters are typically calibrated using experimental observations or quantum mechanical reference data, which are typically obtained from density functional theory (DFT) calculations. Before conducting extensive MD simulations of CO oxidation in scCO₂, a dedicated ReaxFF force field parameter set for CO₂ was developed. All the DFT calculations were

performed in the Amsterdam Modeling Suite (AMS).⁵⁰ Unless otherwise mentioned, all those calculations are done with the B3LYP hybrid exchange-correlation (xc) functional with a TZ2P basis set. We also included second-order Møller-Plesset (MP2) calculations in our training dataset. Some of the MP2 calculations were incorporated from existing literature, while others were performed in GAUSSIAN⁵¹, using 6-311++G** basis sets. The detailed procedures for parameter training are discussed in Section 3. The MD simulations described in Section 3.2 utilized the AMS-ReaxFF solver, whereas those in Section 3.3 employed LAMMPS.⁵² Atomistic visualizations were performed in OVITO.⁵³

To obtain the optimized ReaxFF parameter set that best reproduces the reference data, the parameters yielding the minimum cumulative normalized error were selected. The cumulative normalized error was computed using the following equation:

$$Error = \sum_{i=1}^{n} \left[\frac{x_{i,QM} - x_{i,ReaxFF}}{\sigma} \right]^{2}$$
 (2)

where σ denotes the weighting factor assigned to each data point according to its relative importance in the optimization, n is the total number of data points in the training set, and x represents the target property, mainly, the energy values used in this study. The final ReaxFF parameter set can be found in the Supplementary Information (SI).

3. Results and Discussion

3.1. The Force Field Development

The force field parameter optimization commenced with training against various crystal deformation versus energy equations of state (EOS) data, which included the bulk modulus and stiffness tensor components sourced from the Materials Project.⁵⁴ We employed the lattice parameters, bulk modulus (5 GPa), and stiffness tensor (C) of a cubic CO₂ crystal containing four molecules, as illustrated in Figure 1(a). The CO₂ crystal measures 5.5 Å on each side.

Initially, we subjected the original CO₂ crystal to various deformation types⁵⁵, including volumetric deformations (uniform expansion and compression) as well as different crystal strains,

such as normal and shear strain. The energy related to volumetric deformations was calculated using the Birch-Murnaghan EOS,⁵⁶ while a Taylor expansion⁵⁷ was applied to characterize the energy associated with various crystal strains.

The Birch-Murnaghan EOS, a model describing the relationship between the volume and energy of a crystal under compression or expansion, was used to fit the energy-volume data for isotropically distorted structures of CO₂. Here, the initial structure was uniformly expanded and compressed up to 12% of its original volume. Figure 1(b) depicts the resulting energy vs volume EOS. The third-order Birch-Murnaghan EOS is expressed as:

$$P(V) = \frac{3B_0}{2} \left[\left(\frac{V_0}{V} \right)^{\frac{7}{3}} - \left(\frac{V_0}{V} \right)^{\frac{5}{3}} \right] \left\{ 1 + \frac{3}{4} \left(B_0' - 4 \right) \left[\left(\frac{V_0}{V} \right)^{\frac{2}{3}} - 1 \right] \right\}$$
 (3.1)

where, P (GPa) is the pressure, V (Å³) is the volume, V_{θ} (Å³) is the reference volume at zero pressure, B_{θ} (GPa) is the bulk modulus at zero pressure, B'_{θ} (dimensionless) is the first pressure derivative of the bulk modulus.

The stiffness tensor (C) for the considered crystal is shown in Equation (3.2).

$$C (GPa) = \begin{bmatrix} C11 & C12 & C13 & 0 & 0 & 0 \\ C21 & C22 & C23 & 0 & 0 & 0 \\ C31 & C32 & C33 & 0 & 0 & 0 \\ 0 & 0 & 0 & C44 & 0 & 0 \\ 0 & 0 & 0 & 0 & C55 & 0 \\ 0 & 0 & 0 & 0 & 0 & C66 \end{bmatrix} = \begin{bmatrix} 8 & 3 & 3 & 0 & 0 & 0 \\ 3 & 8 & 3 & 0 & 0 & 0 \\ 3 & 8 & 3 & 0 & 0 & 0 \\ 3 & 8 & 3 & 0 & 0 & 0 \\ 0 & 0 & 0 & 2 & 0 & 0 \\ 0 & 0 & 0 & 2 & 0 & 0 \\ 0 & 0 & 0 & 0 & 2 & 0 \\ 0 & 0 & 0 & 0 & 0 & 2 \end{bmatrix}$$
(3.2)

Here, C11, C22, C33 are the normal stiffness components along the principal axes; C12, C13, C23 are the coupling stiffness components; and C44, C55, C66 are the shear stiffness components. These stiffness tensor components represent the material's response to different types of mechanical strains, critical for understanding the material's elastic behavior. Like the Bulk modulus, we applied different types of strain (5%) to the crystal corresponding to each stiffness tensor component, such as normal strain and shear strain. The energy corresponding to each

deformed structure was generated using the Taylor series expansion. The Taylor expansion for the internal energy $E(V, \delta)$ of a crystal under strain δ up to the second order is given by:

$$E(V,\delta) = E(V_0,0) + V_0 \left(\sum_i \tau_i \delta_i + \frac{1}{2} \sum_i C_{ij} \delta_i \delta_j \right)$$
(3.3)

where, $E(V_0, 0)$ (kcal/mol) is the internal energy of the unstrained crystal, V_0 (Å³) is the reference volume of the unstrained crystal, τ_i (GPa) are the components of the stress tensor, C_{ij} (GPa) are the elastic stiffness constants, δ_i and δ_j (dimensionless) are the strain components.

Figure 1(c) depicts the resulting strain vs energy EOS for C11 stiffness tensor components. The *x*-axis in the graphs represents the percentage and direction of applied strain. The EOSs for other stiffness components are presented in the SI, Figure S1. The objective of training the force field parameters in response to the energy changes associated with crystal deformation is to ensure that the force field accurately reflects the elastic properties of CO₂. Figure 1 indicates that ReaxFF shows considerable accuracy in reproducing the "U-shaped" energy vs deformation profiles. Overall, ReaxFF demonstrates good accuracy for less deformed structures, but deviations rise with higher strain. However, it is important to realize that the ultimate accuracy of the force field is contingent upon the entirety of the training set, rather than any one data set. Each component of the training data is designed to collectively guide the parameters in the appropriate direction.

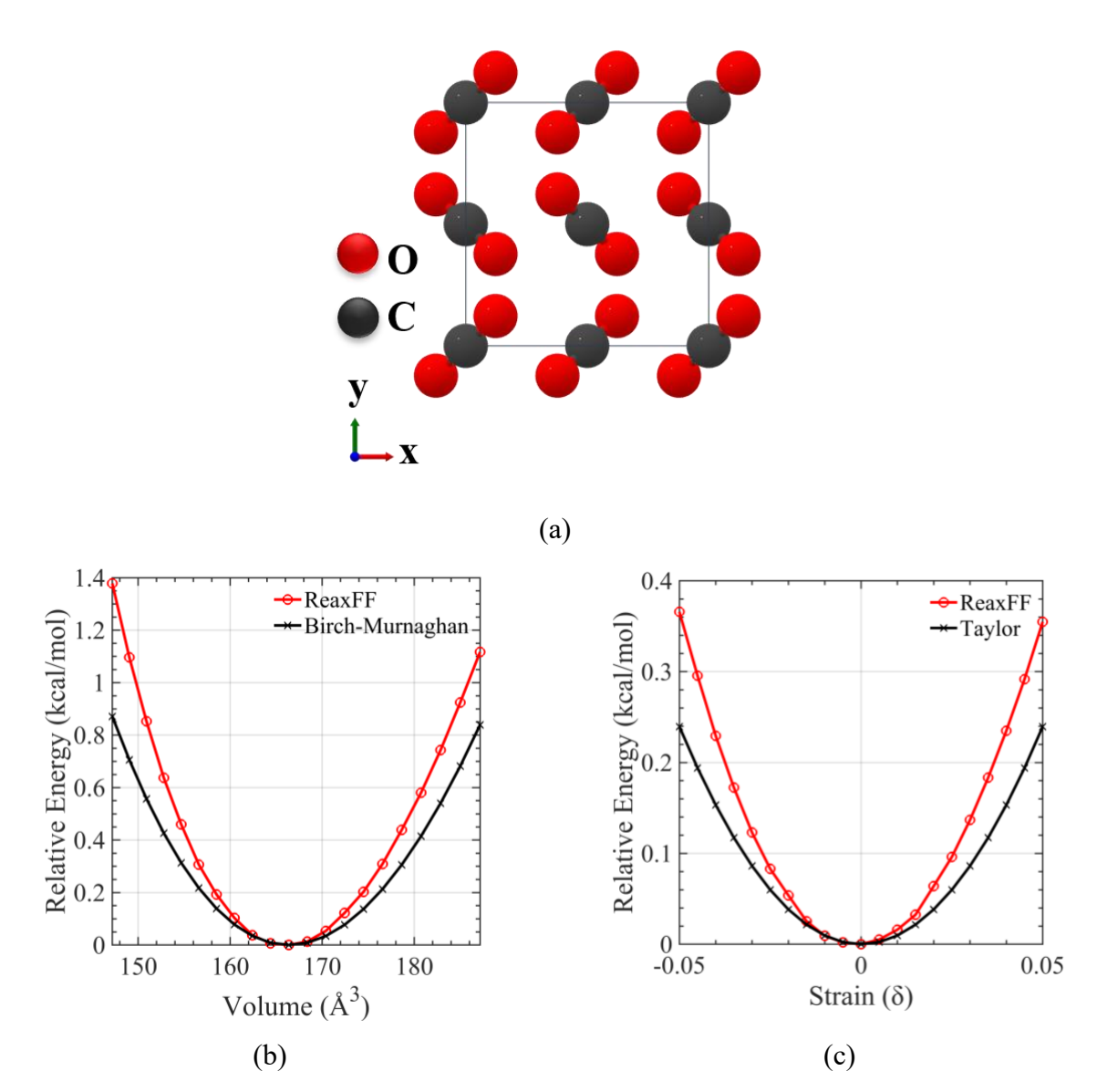


Figure 1. Training ReaxFF against CO₂ crystal equation of states for bulk modulus and stiffness tensor components. Red and gray spheres represent oxygen and carbon atoms, respectively. (a) The cubic CO₂ crystal considered for this calculation; (b) variation of the relative energy as a function of volumetric strain; and (c) variation of the relative energy as a function of normal strain along the x-axis. The energy of the undistorted CO₂ crystal has been taken as the reference for obtaining relative energy values.

To accurately model intermolecular CO₂-CO₂ interactions, we trained our force field against CO₂ dimer energies for both slid-parallel (C_{2h}) dimers (see Figure 2(a)) and cross or Tshaped $(C_{2\nu})$ dimers (see Figure 3(a)) computed by MP2 calculations, obtained from ref. ⁵⁸. These MP2 energy values were calculated using the 6-311+G(2df) basis set, and basis set superposition errors (BSSE) were corrected by the counterpoise method. It is worth noting that C_{2h} and C_{2v} dimers are reported to be the most stable forms of CO₂ dimers.⁵⁸ Figure 2 depicts the comparison of ReaxFF and MP2 energy values for the slid-parallel dimers, where R₁ is the intermolecular C-C distance in the vertical direction, and R₂ is the C-C distance in the horizontal direction. Based on the analysis of Figure 2, the ReaxFF force field demonstrates good performance in predicting the trends of energy-distance profiles. The largest average deviation is observed for dimers with $R_1 = 3.2 \text{ Å}$ (~ 14%), while the smallest average deviation is observed for $R_1 = 3.4 \text{ Å}$ (~ 3%). Similarly, training data for the CO₂ cross or T-shaped dimers, obtained from ref. ⁵⁸, are presented in Figure 3. Figure 3(a) illustrates the T-shaped dimer, and Figure 3(b) shows the relative energy vs C-C distance (R). ReaxFF is found to mimic the shape of the energy profile considerably well. However, ReaxFF exhibits greater accuracy for distances greater than 4.2 Å, while it slightly underpredicts the potential energy between 3.9 Å and 4.2 Å. The average percentage deviation of ReaxFF for the cross-dimer energy is $\sim 10\%$.

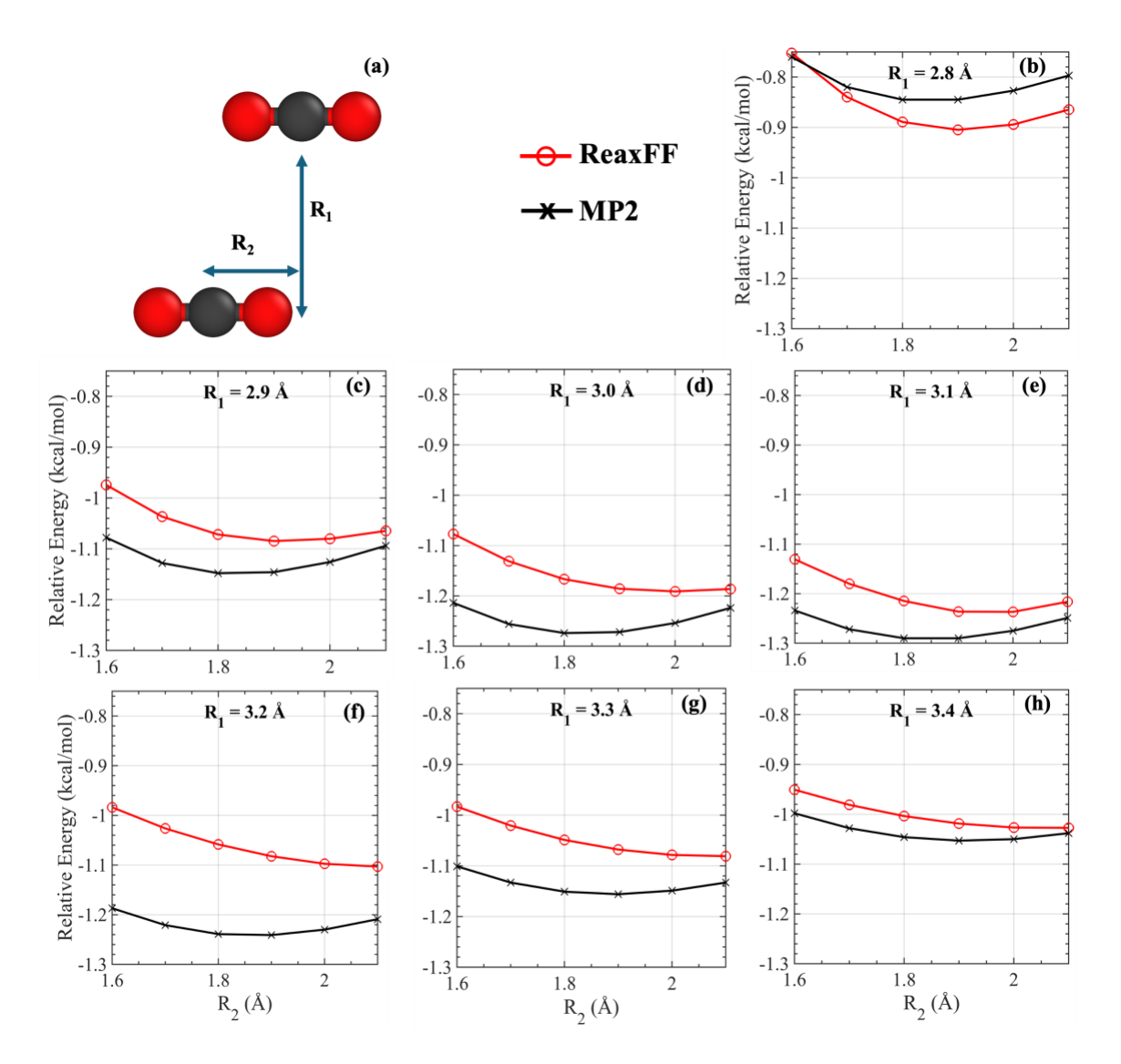


Figure 2. Training ReaxFF against CO₂ slid-parallel dimer computed from MP2 calculations. (a) Geometry of the slid-parallel dimer considered for this calculation. Red and gray spheres represent oxygen and carbon atoms, respectively. R₁ is the vertical C-C distance, and R₂ is the horizontal C-C distance. (b)-(h) Comparison between MP2 and ReaxFF energies. For each plot, the distance R₂ is varied by keeping R₁ fixed (specified inside the plot). The energy of two isolated CO₂ molecules has been taken as the reference for obtaining relative energy values.

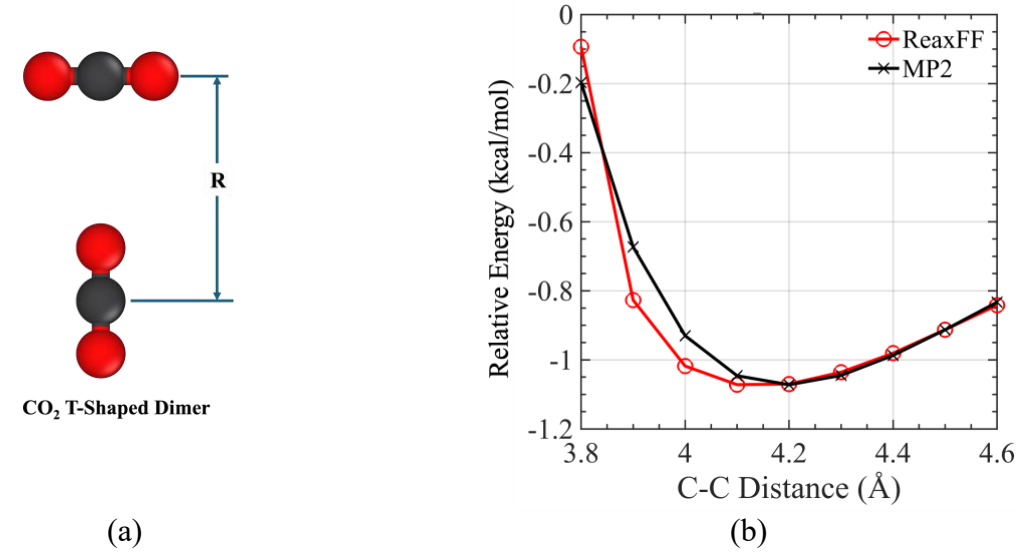


Figure 3. Training ReaxFF against the CO₂ T-shaped dimer computed from MP2 calculations. (a) Configuration of the CO₂ T-shaped dimer. Red and gray spheres represent oxygen and carbon atoms, respectively. The C-C distance is R. (b) Comparison between ReaxFF and MP2 energy vs C-C distance (R). The energy of two isolated CO₂ molecules has been taken as the reference for obtaining relative energy values.

Furthermore, to accurately model the pressure and density of CO₂, it is crucial to correctly account for long-range intermolecular CO₂ interactions. Standard DFT functionals often fail to accurately account for long-range electron correlation effects responsible for van der Waals interactions.^{59,60} This leads to inaccuracies in systems where dispersion forces play a crucial role, such as in molecular dimers. To overcome this issue, more accurate quantum chemical methods, like the MP2 method were used for calculating the CO₂ dimer long-range interactions. Hence, we trained our force field parameters for CO₂ dimer interaction energies from 3 Å – 6 Å for both slid-parallel dimers (Figure 4(a)) and cross dimers (Figure 4(b)) using GAUSSIAN, MP2 calculations with 6-311++G** basis sets. In general, ReaxFF slightly underpredicts the stability for parallel dimers, and the accuracy of ReaxFF improves when the C-C distance exceeds 5 Å. Alternatively, ReaxFF shows an excellent agreement in predicting energy for cross dimers; however, the

deviation increases when the C-C distance goes beyond 4 Å. For the parallel dimers, the ReaxFF energy values exhibit an average deviation of $\sim 11\%$, whereas for the cross dimers, the average deviation is $\sim 5\%$.

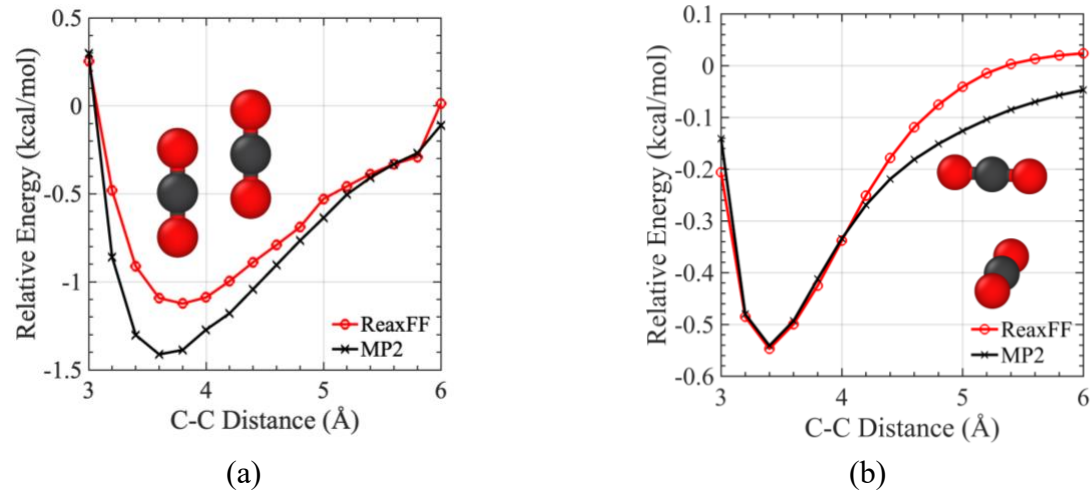


Figure 4. Training ReaxFF against CO₂ parallel and cross dimer interactions from MP2 calculations. (a) Comparison of ReaxFF and MP2 energies for the parallel dimers. (b) Comparison between ReaxFF and MP2 energy for cross dimers. Red and gray spheres represent oxygen and carbon atoms, respectively. The energy of two isolated CO₂ molecules has been taken as the reference for obtaining relative energy values.

Moreover, to suppress unphysical CO₂ dimerization to C₂O₄ during MD simulations, it was necessary to train the force field to have a high dimer formation energy barrier and to correctly predict the endothermicity of this reaction. To achieve this, we trained the force field against the DFT-predicted CO₂ dimer formation reaction pathway, see Figure 5(a). For this training, the intermolecular C-O distance was varied from 4 Å to 1.2 Å (indicated with a double-headed arrow in Figure 5(a)), and the potential energy of seventeen intermediate points was calculated. The DFT calculations were performed using the B3LYP hybrid xc functional with the TZ2P basis set. The DFT estimated dimerization energy barrier was approximately 50 kcal/mol. Figure 5(a) illustrates that ReaxFF traces the energy barrier with sufficient accuracy, indicating that unwanted

dimerization is highly improbable. The ReaxFF-predicted energy barrier was approximately 57 kcal/mol. Figure 5(a) also indicates that ReaxFF slightly overpredicts the attraction energy of dimers between 2.6 Å and 3.2 Å compared to DFT. Below 2.6 Å, the ReaxFF energy graph becomes steeper than the DFT graph, indicating a rapid increase in the repulsive energy.

Previous experimental and theoretical investigations indicated that short-lived carbon trioxide (CO₃) may form under certain conditions through the interaction of O with CO₂.^{61–65} Its formation has been experimentally observed under specific conditions, such as during ozone photolysis in liquid CO₂⁶³ and within low-temperature solid CO₂ exposed to electron irradiation.^{64,65} Despite its brief existence, the production route of CO₃ is pertinent to atmospheric phenomena, including O(¹D) quenching and isotope exchange.^{64,65} Therefore, accurately capturing the energetics of the CO₃ formation reaction was considered important for the accuracy of our ReaxFF force field. Hence, we trained the force field against the CO₃ formation energy. We gradually reduced the distance between an O radical and the C atom of a CO₂ molecule and used the energy profile obtained from DFT to train ReaxFF. For this DFT calculation, we used the hybrid B3LYP functional with the QZ4P basis set. Figure 5(b) illustrates the trained force field predicting the reaction path for CO₃ formation accurately.

To aid the force field in predicting the O₂ binding energy, we trained it for both the O=O double bond and O-O single bond energies, as shown in Figures 5(c) and 5(d), respectively. For the O=O double bond energy, we varied the interatomic distance between two oxygen atoms, and for the O-O single bond energy, we adjusted the O-O distance between two oxygen atoms in an H₂O₂ molecule. The trained force field can accurately predict O₂ bond energies. Further, we trained the force field for the C=O triple bond distance vs energy data for the carbon monoxide molecule, computed from DFT calculations. As manifested in Figure 5(e), the trained force field exhibits

excellent agreement with the reference DFT data in reproducing the single-well-shaped energy profile. The average deviation of ReaxFF from the DFT data is ~6.4%.

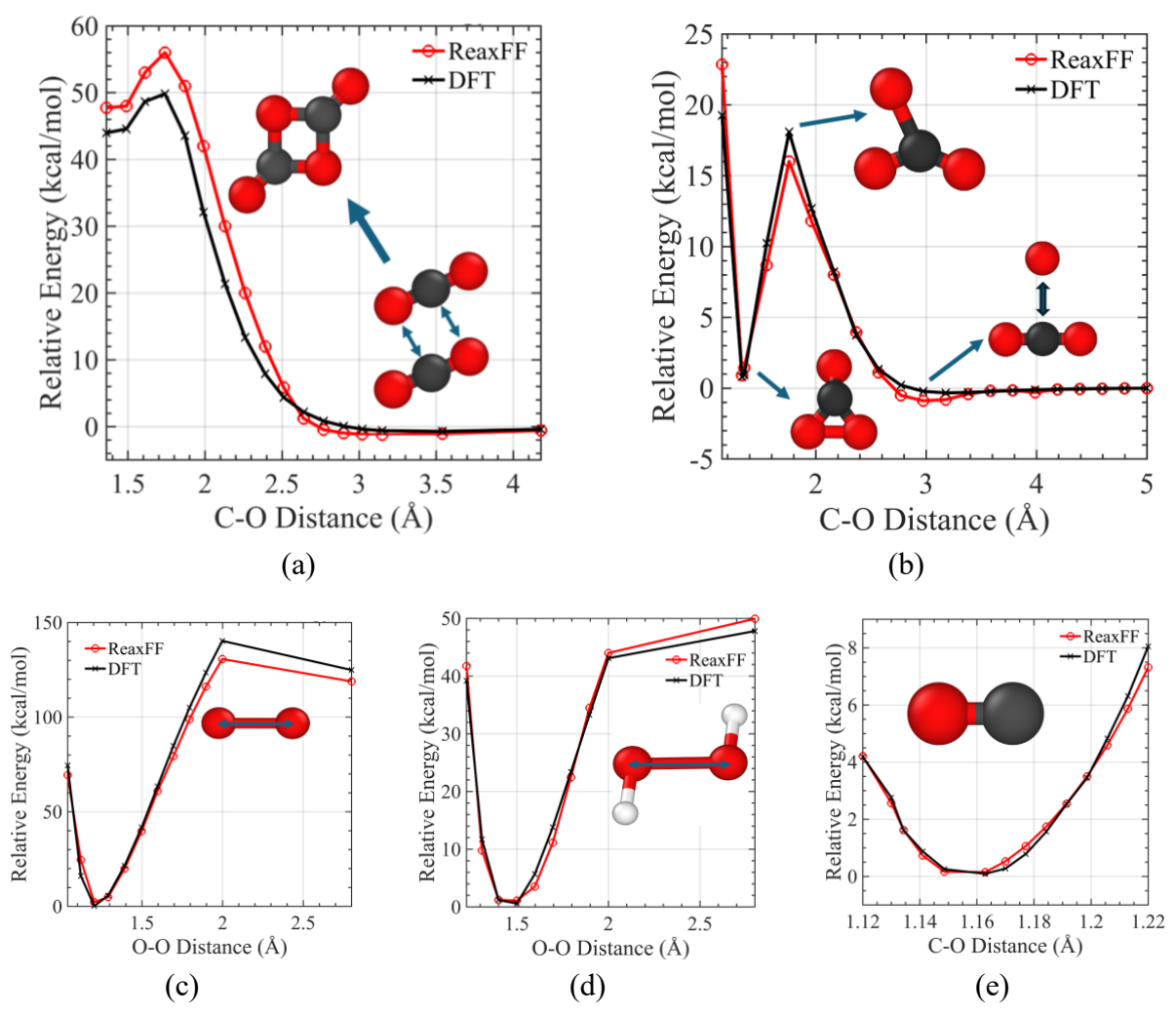


Figure 5. (a) Comparison between ReaxFF and DFT for CO₂-CO₂ dimer formation energy.

CO₂ molecules were brought close to each other by reducing the intermolecular C-O distance, as shown with a double-headed arrow. The energy of two isolated CO₂ molecules has been taken as the reference for obtaining relative energy values. (b) Comparison between ReaxFF and DFT for the CO₃ formation energy, where a CO₂ molecule and O radical were brought close to each other by reducing the intermolecular C-O distance, as shown with a black double-headed arrow. The energy of an isolated CO₂ and an O radical has been taken as the reference for obtaining relative energy values. (c) Comparison between ReaxFF and DFT for the O=O double bond energy. (d)

Comparison between ReaxFF and DFT for the O-O single bond energy. (e) Comparison between ReaxFF and DFT for the C≡O triple bond energy. For (c)-(e), the energy of the most stable O₂, H₂O₂, and CO molecules has been taken as reference energy values, respectively. Red, gray, and white spheres represent oxygen, carbon, and hydrogen atoms, respectively.

We also trained our force field for the cohesive energy of solid CO₂ obtained from existing literature, ⁶⁶ where authors utilized an incrementally corrected periodic local MP2 (LMP2) scheme with post-MP2 CCSD(T) corrections and basis-set limit extrapolation. Cohesive energy is a fundamental property that indicates the strength of the interactions holding a solid together. It was calculated as the difference between the potential energy of solid CO₂ and the sum of the energies of its isolated constituent molecules. This energy is crucial for understanding the stability, binding strength, and various physical properties of materials, like hardness, melting point, mechanical strength, and phase transitions. The ReaxFF predicted CO₂ cohesive energy is approximately -7.1 kcal/mol, while the literature value is approximately -7.05 kcal/mol.⁶⁶ This good agreement between ReaxFF and literature cohesive energy helps ensure that the developed force field accurately captures the essential intermolecular forces and the overall stability of the CO₂ crystal structure.

To further improve the density and pressure prediction of the force field, we recognized the need to train it for larger CO₂ clusters. However, performing QM calculations for a large system is computationally infeasible. Therefore, we conducted NPT simulations at 10 MPa and 316 K (scCO₂) with a system of 25 CO₂ molecules and another system containing 50 CO₂ molecules using the Cygan potential⁶⁷ for 3 ns with a 0.25 fs time-step so that the systems reach equilibrium at the supercritical state. We then systematically expanded and compressed the final geometries to generate systems with varying densities from vapor to solid zones (0.14 g/cm³ - 1.8 g/cm³). This

provides short and long-range interactions of CO₂ molecules in a larger system. Afterward, we energy minimized each geometry using the conjugate gradient scheme and calculated the energy versus density EOS for those systems using the Cygan potential, and trained ReaxFF parameters against those values. It is worth mentioning that the Cygan potential is a three-site flexible force field⁶⁷ and generally performs well in predicting CO₂ density and interactions, particularly excelling in predicting the self-diffusion coefficient and showing reasonable accuracy in structural predictions through RDF analysis.^{68–70} Figures 6(a) and 6(b) show the energy vs. density EOS comparison between ReaxFF and the Cygan potential for the 25 CO₂ and 50 CO₂ systems, respectively. As expected, as the density increases from vapor to solid, the potential energy decreases continuously due to the stronger intermolecular attraction. The equilibrium density of a CO₂ crystal is ~1.52 g/cm³.⁵⁴ Hence, further compression beyond this point increases the potential energy values. For the 25 CO₂ system, the average deviation of ReaxFF is ~9%, while it is ~3% for the 50 CO₂ system.

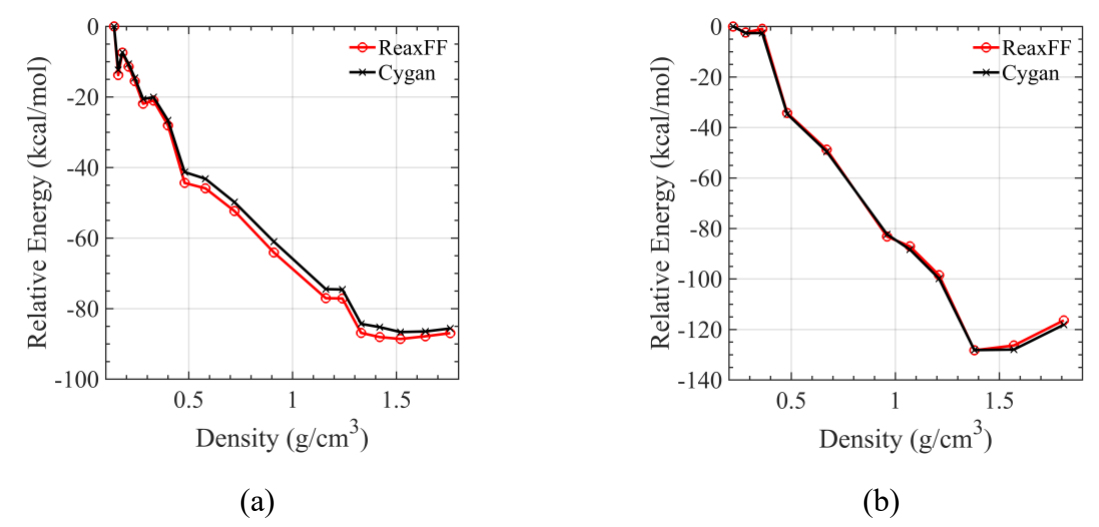
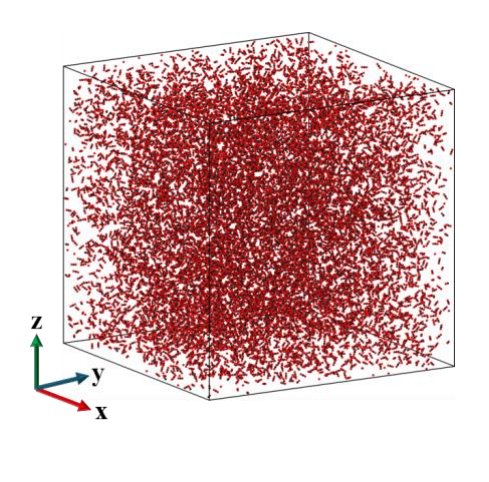
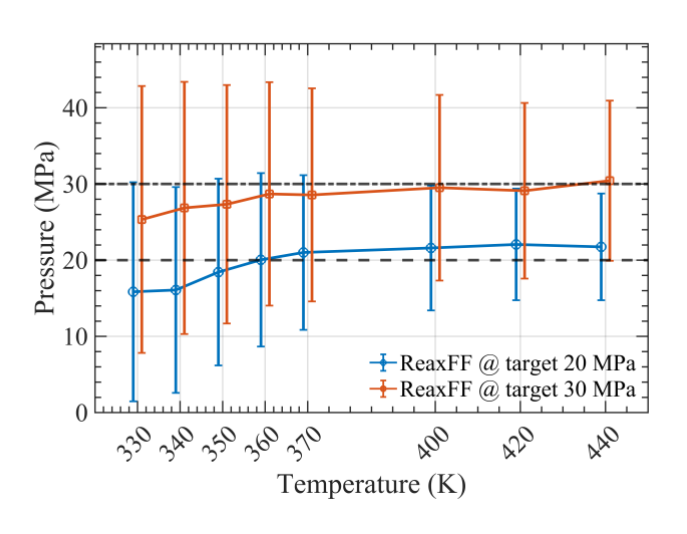


Figure 6. Training ReaxFF against energy vs density EOS calculated from Cygan force field for: (a) a system of 25 CO₂; (b) a system of 50 CO₂.

3.2. Testing Force Field Performance

To evaluate the fidelity of our CO₂ ReaxFF description for predicting the CO₂ non-reactive phase diagram, we performed canonical-ensemble (NVT) MD in the supercritical regime (330-440 K). The MD simulations were run for 2 ns with a time step of 0.25 fs to ensure the systems reached equilibrium. For all simulations, we employed a temperature-damping constant of 100 fs. Equilibrium pressures were subsequently calculated by averaging the densities over the last 1 ns of the simulations. For each temperature, two initial configurations with 11,000 CO₂ molecules were prepared with densities taken from the National Institute of Standards and Technology (NIST)⁷¹ data along the 20 and 30 MPa isobars. After equilibration at the target temperature, we computed the time-averaged system pressure and compared it directly to the corresponding NIST target (20 or 30 MPa) to quantify deviations. Figure 7(a) illustrates the configuration of supercritical CO₂ (11,000 molecules) in the simulation cell. Figure 7(b) depicts the ReaxFF equilibrium pressure versus temperature (330-440 K) for systems initialized at NIST densities on the 20 MPa (blue) and 30 MPa (orange) isobars. Symbols show time-averaged pressure with standard deviation. The corresponding NIST targets are presented with horizontal dashed lines.



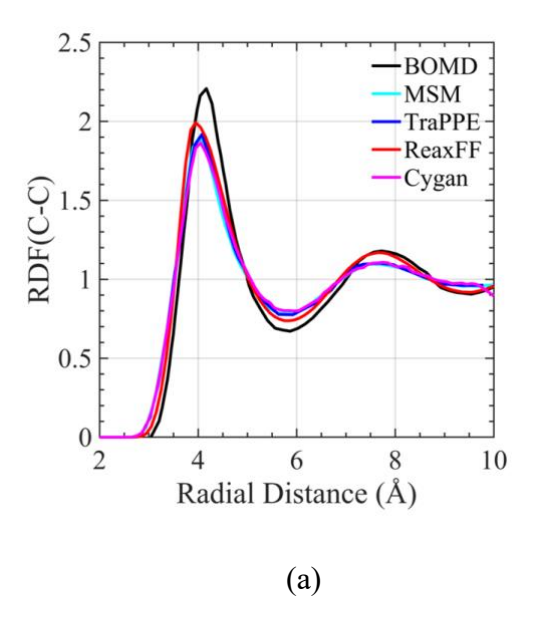


(a) (b)

Figure 7. (a) Representation of supercritical CO₂ (11,000 molecules) in a simulation cell. (b) ReaxFF equilibrium pressure versus temperature for systems initialized at NIST densities on the 20 MPa (blue) and 30 MPa (orange) isobars. Symbols show time-averaged pressure with standard deviation. Horizontal dashed lines indicate the corresponding NIST targets.

The radial distribution function (RDF) is a critical tool in structural analysis, offering detailed insights into the spatial arrangement of atoms or molecules within a material. For CO₂, the RDF describes how the density of CO₂ molecules varies as a function of distance from a reference molecule, providing essential information about the short-range and long-range order in the system. By calculating the RDF, we can identify the most probable distances between pairs of CO₂ molecules, which correspond to peaks in the RDF plot.

In Figures 8(a-b), we calculated the RDF of CO₂ using ReaxFF for a liquid CO₂ system at 233 K (density = 1.08 g/cm³) and a supercritical CO₂ (scCO₂) system at 315 K (density = 0.81 g/cm³), and compared them with other force fields, such as Born-Oppenheimer molecular-dynamics (BOMD), MSM, and TraPPE from existing literature.⁷² We also performed simulations with the Cygan potential to compare RDF against ReaxFF. For both ReaxFF and the Cygan potential, simulations were performed with 108 CO₂ molecules (same as ref.⁷²) under the canonical ensemble (NVT) for 1 ns with a time step of 0.25 fs. The average RDF was then calculated by averaging RDFs over the last 500 ps to minimize noise. It was found that ReaxFF shows excellent agreement in predicting the RDF compared to other interatomic potentials. Such a comparison with published literature ensures that the new force field accurately reproduces the known structural characteristics of CO₂, confirming its reliability and effectiveness in capturing the intricate details of molecular interactions and arrangements.



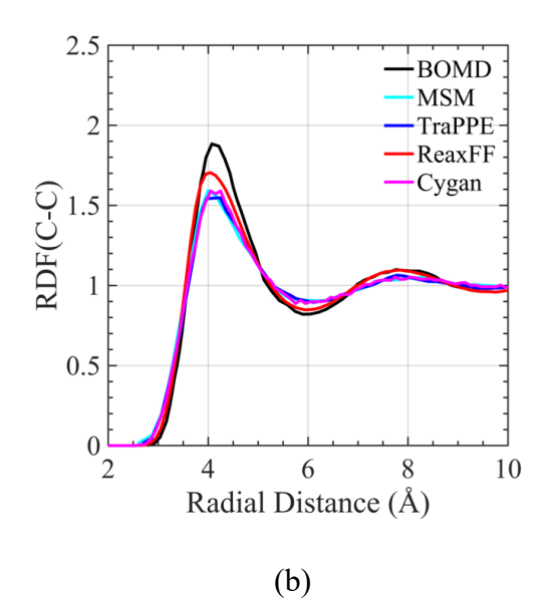


Figure 8. Comparison of CO_2 radial distribution function (C-C pair) between ReaxFF and other non-reactive force fields. (a) Radial distribution function plot for liquid CO_2 at 233 K (system density = 1.08 g/cm³). (b) Radial distribution function plot for supercritical CO_2 at 315 K (system density = 0.81 g/cm³).

3.3. ReaxFF Modeling of CO Oxidation in Supercritical CO2

As mentioned earlier, in heavily backmixed CO-air systems and in high-temperature oxyfuel or $scCO_2$ flames, the O radical directly facilitates CO oxidation, $^{14,18-21}$ and one of our objectives is to investigate this phenomenon with our developed ReaxFF force field. It is worth noting that the production of CO_2 from CO and O is a highly exothermic reaction that releases energy in the form of heat. Consequently, freshly generated CO_2 can obtain a significant amount of kinetic energy (KE), distributed over translational, rotational and vibrational modes. If the vibrational KE of CO_2 obtained exceeds the bond dissociation energy (BDE) of CO_2 ($CO_2 \rightarrow CO + O$), which is approximately 125.73 kcal/mol (at 0 K), 73 CO_2 can dissociate back into CO + O.

To investigate this phenomenon, a system comprising 20 CO molecules and 20 O atoms was considered within a 20 Å x 20 Å x 20 Å simulated box, yielding a system density of 0.18 g/cm³. Subsequently, we conducted MD simulation within the microcanonical ensemble (NVE) for 1 ns, with a time step of 0.05 fs. It is noteworthy that systems containing radicals, such as O, need a reduced time step due to high local temperatures. We noted that the collision of CO and O resulted in the formation of numerous transient CO₂ molecules, which subsequently dissociated

back into CO and O. Specifically, when CO₂ is created, if it is unable to disperse the substantial energy produced through collisions, one of the two oxygen atoms may detach from the CO₂ molecule. Figure 9(a) illustrates that the collision between a CO molecule and an O radical resulted in the formation of one CO₂ molecule. The oxygen originally bound to the carbon atom is designated as O(1), whereas the initial oxygen radical is designated as O(2). The freshly produced CO₂ could not achieve stability and ultimately dissociates again. However, the initially bound O(1) becomes separated this time. Figures 9(b) and 9(c) illustrate the variations in KE and total energy of the initial CO(1) molecule prior to and subsequent to the impact, respectively. The CO(1) molecule collides with the O(2) molecule at around 21.5 ps, resulting in the detachment of the O(1) atom from the newly formed CO₂ molecule at around 22.5 ps. Subsequent to the impact, the KE of the CO(1) molecule increases by ~180 kcal/mol, surpassing the aforementioned BDE. Consequently, the CO(1) bond breaks. During the simulated period, CO₂ was continuously created and dissociated, resulting in a low level of stable CO₂ production. Therefore, it may be concluded that in a dilute environment, the conversion of CO and O into CO₂ is not efficient.

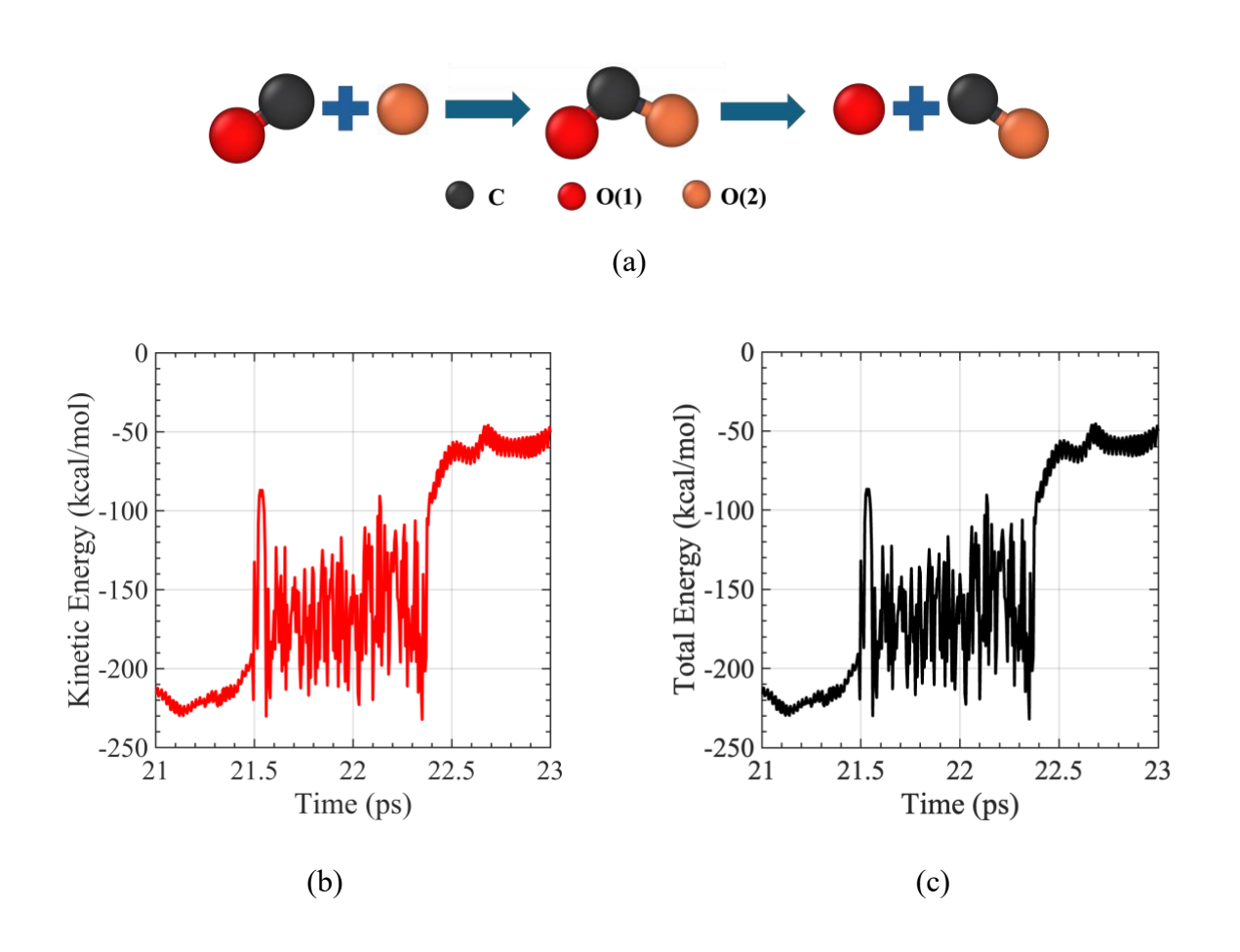


Figure 9. (a) Reaction of CO + O in a dilute system. The black sphere represents a C atom; the red sphere represents the O atom in the initial CO molecule (O(1)); the orange sphere represents an isolated O radical (O(2)). The newly generated CO_2 from this reaction did not sustain due to the large amount of KE generated due to the collision, and the initially bonded O(1) dislodged from the molecule. (b) and (c) represent kinetic and total energy changes of the initial CO(1) molecule before and after the collision, respectively.

Consecutively, we investigated the CO + O reaction under an scCO₂ atmosphere. We initially utilized a system of 400 CO₂ molecules with a starting density of 0.843 g/cm³ and conducted an NVT simulation at 330 K, employing a time step of 0.25 fs and a damping time of 100 fs. At equilibrium, the mean pressure of the system reached 25.3 MPa, and this pressure and temperature combination corresponds to the supercritical state of CO₂.⁷¹ Afterward, 20 CO molecules and 20 O radicals were randomly added into the scCO₂ system. We then simulated the reactants (CO + O) under the NVE ensemble, while regulating the solvent molecules (CO₂) at 330 K by a weak thermostat with a temperature damping constant of 1000 fs. The simulation was performed for 2 ns with a time step of 0.05 fs. Approximately 200 ps later, eight more stable CO₂ molecules were produced in the system, and after 2 ns, a total of eleven new CO₂ molecules were identified. The newly formed CO₂ molecules were observed to dissipate excess vibrational KE through continuous collisions with the surrounding scCO₂ matrix.

Figure 10 illustrates a representative collision event that contributed to the stabilization of a nascent CO₂ molecule. Figure 10(a) provides a snapshot highlighting the newly formed CO₂ (yellow) and its neighbors (green). Note that, in this context, neighbors are defined as species located within a 4 Å distance from the nascent CO₂ at a specific time. The subsequent plots quantify the energy exchange during a 1.5 ps window. Figure 10(b) portrays a reduction of ~80 kcal/mol in the total energy of the new CO₂ molecule after collisions, whereas Figure 10(c) depicts a corresponding energy increase of ~70 kcal/mol in the neighboring molecules. The little discrepancy in energy change between the new CO₂ and its neighbors occurs due to the simultaneous energy exchange of these neighbors with their own surroundings. This observation, in which the dense supercritical solvent aids in stabilizing highly energetic products from exothermic reactions by collisional energy transfer, is consistent with prior ReaxFF studies, including the research of Mirakhori *et al.* ⁴⁸ on iodine recombination in supercritical xenon matrix. Our atomistic demonstration that newly formed CO₂ is stabilized via collisional energy transfer to

the dense scCO₂ environment yields important mechanistic insight for combustion kinetics and supercritical reactor design.

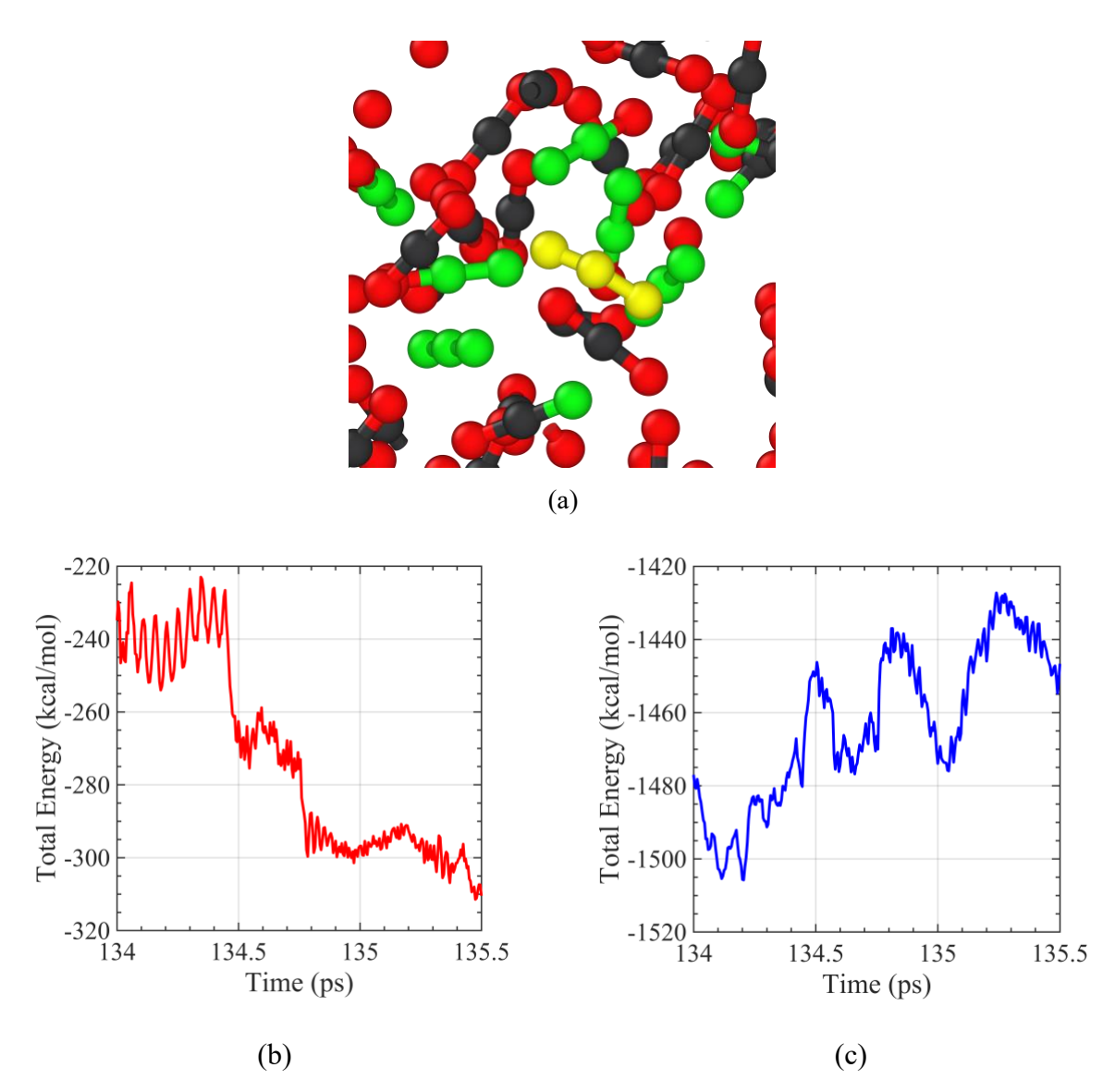


Figure 10. (a) Snapshot of a nascent CO₂ along with its neighbors. The new CO₂ is highlighted with yellow color, and its neighbors within 4 Å distances are highlighted in green. (b) Total energy changes of a newly formed CO₂ molecule during a collision with neighbors. (c) Total energy changes of 10 neighboring molecules of the newly formed CO₂.

Conclusions

In this study, we developed and utilized a new ReaxFF reactive force field to investigate the atomistic mechanism of the CO + O reaction in a supercritical CO₂ (scCO₂) environment. The

force field parameters were trained using a comprehensive set of quantum mechanical (QM) data. The resulting model demonstrated excellent agreement with the reference values. The force field was found to reproduce the pressure behavior of bulk scCO₂ with reasonable accuracy when compared to NIST data. Furthermore, comparisons of the radial distribution function (RDF) for both liquid and scCO₂ showed strong accordance with other published non-reactive force fields, confirming the structural accuracy of ReaxFF. Utilizing this novel force field, we observed that the formation of CO₂ from the CO+O reaction in a dilute system is highly inefficient. The high exothermicity of the reaction results in significant kinetic energy transfer to the newly formed CO₂ molecule, which leads to its rapid dissociation without a third body to absorb the energy. However, when a similar reaction was modelled in a dense scCO₂ environment, the surrounding molecules functioned as an effective stabilizing medium. The newly formed, high-energy CO₂ product transferred its excess energy through collisions with the solvent, leading to stability. The findings emphasize the active role of the supercritical CO₂ in stabilizing exothermic products and are anticipated to be valuable to the scientific community focused on combustion and high-pressure systems.

Acknowledgments

The work was supported by the U.S. Department of Energy under contract No. DE-SC0022222. ACTvD and YS acknowledge funding from the Office of Naval Research Grant through Grant No. N00014-23-1-2725. The ReaxFF MD simulations were performed on the Roar supercomputer managed by the Penn State Institute for Computational and Data Sciences.

References

- Knez, Ž. et al. Industrial applications of supercritical fluids: A review. Energy 77, 235–243 (2014).
- Parhi, R. & Suresh, P. Supercritical Fluid Technology: A Review. J. Adv. Pharm. Sci. Technol. 1, 13–36 (2013).

- Machado, B. A. S., Pereira, C. G., Nunes, S. B., Padilha, F. F. & Umsza-Guez, M. A.
 Supercritical Fluid Extraction Using CO2: Main Applications and Future Perspectives. Sep. Sci. Technol. 48, 2741–2760 (2013).
- 4. Manjare, S. D. & Dhingra, K. Supercritical fluids in separation and purification: A review. *Mater. Sci. Energy Technol.* **2**, 463–484 (2019).
- 5. Ahn, Y. *et al.* Review of supercritical CO2 power cycle technology and current status of research and development. *Nucl. Eng. Technol.* **47**, 647–661 (2015).
- White, M. T., Bianchi, G., Chai, L., Tassou, S. A. & Sayma, A. I. Review of Supercritical CO2 Technologies and Systems for Power Generation. *Appl. Therm. Eng.* 185, 116447 (2021).
- 7. Munshi, P. & Bhaduri, S. ChemInform Abstract: Supercritical CO₂ A Twenty-First Century Solvent for the Chemical Industry. *ChemInform* **41**, chin.201011250 (2010).
- de Castro, M. D. L., Valcárcel, M. & Tena, M. T. Physico Chemical Properties of Supercritical Fluids. in *Analytical Supercritical Fluid Extraction* (eds de Castro, M. D. L., Valcárcel, M. & Tena, M. T.) 32–78 (Springer, Berlin, Heidelberg, 1994). doi:10.1007/978-3-642-78673-0 2.
- 9. Nikolai, P., Rabiyat, B., Aslan, A. & Ilmutdin, A. Supercritical CO2: Properties and Technological Applications A Review. *J. Therm. Sci.* **28**, 394–430 (2019).
- 10. Mao, Q. *et al.* Classical and reactive molecular dynamics: Principles and applications in combustion and energy systems. *Prog. Energy Combust. Sci.* **97**, 101084 (2023).
- 11. Quantum Chemical Study of Supercritical Carbon Dioxide Effects on Combustion Kinetics | The Journal of Physical Chemistry A. https://pubs.acs.org/doi/full/10.1021/acs.jpca.7b02638.

- 12. Bowman, C. T. Kinetics of pollutant formation and destruction in combustion. *Prog. Energy Combust. Sci.* **1**, 33–45 (1975).
- 13. Chester, A. W. Chapter 6 CO combustion promoters: past and present. in *Studies in Surface Science and Catalysis* (ed. Ocelli, M. L.) vol. 166 67–77 (Elsevier, 2007).
- Sabatino, F. D., Connolly, B. J., Pryor, O. M. & White, S. H. Perspectives on oxy-fuel combustion for supercritical CO2 direct-fired power cycle. *Appl. Energy Combust. Sci.* 20, 100297 (2024).
- 15. Bowman, C. T. Kinetics of pollutant formation and destruction in combustion. *Prog. Energy Combust. Sci.* **1**, 33–45 (1975).
- Gonzalo-Tirado, C. & Jiménez, S. Detailed analysis of the CO oxidation chemistry around a coal char particle under conventional and oxy-fuel combustion conditions. *Combust. Flame* 162, 478–485 (2015).
- 17. An Introduction to Combustion: Concepts and Applications.
- 18. Molecular Dynamics Study of Combustion Reactions in a Supercritical Environment. Part 2: Boxed MD Study of CO + OH → CO2 + H Reaction Kinetics | The Journal of Physical Chemistry A. https://pubs.acs.org/doi/full/10.1021/acs.jpca.7b09774.
- 19. Manikantachari, K. R. V., Martin, S., Rahman, R. K., Velez, C. & Vasu, S. A General Study of Counterflow Diffusion Flames for Supercritical CO2 Combustion. *J. Eng. Gas Turbines Power* **141**, (2019).
- 20. Yetter, R. A., Dryer, F. L. & Rabitz, H. Complications of one-step kinetics for moist CO oxidation. *Symp. Int. Combust.* **21**, 749–760 (1988).

- 21. Gonzalo-Tirado, C. & Jiménez, S. Detailed analysis of the CO oxidation chemistry around a coal char particle under conventional and oxy-fuel combustion conditions. *Combust. Flame* 162, 478–485 (2015).
- 22. Singh, S. A. & Madras, G. Detailed mechanism and kinetic study of CO oxidation on cobalt oxide surfaces. *Appl. Catal. Gen.* **504**, 463–475 (2015).
- 23. Howard, J. B., Williams, G. C. & Fine, D. H. Kinetics of carbon monoxide oxidation in postflame gases. *Symp. Int. Combust.* **14**, 975–986 (1973).
- 24. MALTE, P. C. & PRATT, D. T. The Role of Energy-Releasing Kinetics in NOx Formation: Fuel-Lean, Jet-Stirred CO-Air Combustion. *Combust. Sci. Technol.* **9**, 221–231 (1974).
- 25. Saharay, M. & Balasubramanian, S. Ab initio molecular-dynamics study of supercritical carbon dioxide. *J. Chem. Phys.* **120**, 9694–9702 (2004).
- Balasubramanian, S., Kohlmeyer, A. & Klein, M. L. Ab initio molecular dynamics study of supercritical carbon dioxide including dispersion corrections. *J. Chem. Phys.* 131, 144506 (2009).
- 27. Zhang, M., Dou, M., Wang, M. & Yu, Y. Study on the solubility parameter of supercritical carbon dioxide system by molecular dynamics simulation. *J. Mol. Liq.* **248**, 322–329 (2017).
- 28. Masunov, A. E., Atlanov, A. A. & Vasu, S. S. Molecular Dynamics Study of Combustion Reactions in a Supercritical Environment. Part 1: Carbon Dioxide and Water Force Field Parameters Refitting and Critical Isotherms of Binary Mixtures. *Energy Fuels* 30, 9622–9627 (2016).
- Azizpour, H., Moradi, M., AsHab, M. & Moradi, H. Prediction of supercritical carbon dioxide solubility parameter using molecular dynamics simulation and developed models. *J. Mol. Lig.* 437, 128492 (2025).

- 30. Li, X., Yang, D., Sun, X. & Zhang, Y. Characterization of phase structures of a supercritical water/supercritical carbon dioxide/heavy oil system with molecular dynamics simulations. *Geoenergy Sci. Eng.* **228**, 211957 (2023).
- 31. Yoo, J.-H., Breitholz, A., Iwai, Y. & Yoo, K.-P. Diffusion coefficients of supercritical carbon dioxide and its mixtures using molecular dynamic simulations. *Korean J. Chem. Eng.* **29**, 935–940 (2012).
- 32. Panteleev, S. V., Masunov, A. E. & Vasu, S. S. Molecular Dynamics Study of Combustion

 Reactions in a Supercritical Environment. Part 2: Boxed MD Study of CO + OH → CO2 + H

 Reaction Kinetics. *J. Phys. Chem. A* 122, 897–908 (2018).
- Monge-Palacios, M., Grajales-González, E. & Sarathy, S. M. Methanol oxy-combustion and supercritical water oxidation: A ReaxFF molecular dynamics study. *Energy* 283, 129104 (2023).
- 34. Chenoweth, K., van Duin, A. C. T. & Goddard, W. A. ReaxFF Reactive Force Field for Molecular Dynamics Simulations of Hydrocarbon Oxidation. J. Phys. Chem. A 112, 1040– 1053 (2008).
- 35. Shin, Y. K., Ashraf, C. M. & van Duin, A. C. T. Development and Applications of the ReaxFF Reactive Force Field for Biological Systems. in *Computational Materials*, *Chemistry, and Biochemistry: From Bold Initiatives to the Last Mile* (eds Shankar, S., Muller, R., Dunning, T. & Chen, G. H.) 157–182 (Springer International Publishing, Cham, 2021). doi:10.1007/978-3-030-18778-1_9.
- 36. Senftle, T. P. *et al.* The ReaxFF reactive force-field: development, applications and future directions. *Npj Comput. Mater.* **2**, 1–14 (2016).

- 37. Dasgupta, N., Shin, Y. K., Fedkin, M. V. & van Duin, A. ReaxFF molecular dynamics simulations of electrolyte–water systems at supercritical temperature. *J. Chem. Phys.* **152**, 204502 (2020).
- 38. Nian, Y., Zhang, H., Zhang, J. & Han, Y. ReaxFF molecular dynamics for pollution degradation and resourcization in the supercritical water system. *Chem. Eng. Process. Process Intensif.* **204**, 109933 (2024).
- 39. Ai, L., Huang, H., Zhou, Y., Chen, M. & Lü, Y. The oxidation of Fe/Ni alloy surface with supercritical water: A ReaxFF molecular dynamics simulation. *Appl. Surf. Sci.* **553**, 149519 (2021).
- 40. Han, Y., Ma, T., Chen, F., Li, W. & Zhang, J. Supercritical water gasification of naphthalene over iron oxide catalyst: A ReaxFF molecular dynamics study. *Int. J. Hydrog. Energy* **44**, 30486–30498 (2019).
- Chenoweth, K., van Duin, A. C. T. & Goddard, W. A. ReaxFF Reactive Force Field for Molecular Dynamics Simulations of Hydrocarbon Oxidation. *J. Phys. Chem. A* 112, 1040– 1053 (2008).
- 42. Castro-Marcano, F., Russo, M. F., van Duin, A. C. T. & Mathews, J. P. Pyrolysis of a large-scale molecular model for Illinois no. 6 coal using the ReaxFF reactive force field. *J. Anal. Appl. Pyrolysis* **109**, 79–89 (2014).
- 43. Xiao, Y., Zeng, J.-F., Liu, J.-W., Lu, X. & Shu, C.-M. Reactive force field (ReaxFF) molecular dynamics investigation of bituminous coal combustion under oxygen-deficient conditions. *Fuel* **318**, 123583 (2022).

- 44. Ashraf, C. & van Duin, A. C. T. Extension of the ReaxFF Combustion Force Field toward Syngas Combustion and Initial Oxidation Kinetics. *J. Phys. Chem. A* **121**, 1051–1068 (2017).
- 45. Zhou, J., Yang, Y. & Yu, Y. ReaxFF molecular dynamics investigation on the oxidation mechanism of Fe surface in supercritical CO2 mixed with O2. *J. CO2 Util.* **65**, 102224 (2022).
- 46. Qiu, Y., Zhong, W., Shao, Y. & Yu, A. Reactive force field molecular dynamics (ReaxFF MD) simulation of coal oxy-fuel combustion. *Powder Technol.* **361**, 337–348 (2020).
- 47. Grajales-González, E., Monge-Palacios, M. & Sarathy, S. M. Atomistic simulations of syngas oxy-combustion in supercritical CO2. *J. CO2 Util.* **49**, 101554 (2021).
- 48. Mirakhory, M., Majumdar, A., Ihme, M. & van Duin, A. C. T. Iodine recombination in xenon solvent: Clusters in the gas to liquid-like state transition. *J. Chem. Phys.* **162**, 194309 (2025).
- 49. O'Hearn, K. A. *et al.* Optimization of the Reax force field for the lithium–oxygen system using a high fidelity charge model. *J. Chem. Phys.* **153**, 084107 (2020).
- 50. Amsterdam Modeling Suite. SCM https://www.scm.com/amsterdam-modeling-suite/.
- 51. Density Functional (DFT) Methods | Gaussian.com. https://gaussian.com/dft/.
- 52. LAMMPS Molecular Dynamics Simulator. https://www.lammps.org/#gsc.tab=0.
- 53. OVITO Scientific data visualization and analysis software. *OVITO* https://www.ovito.org.
- 54. mp-20066: CO2 (Cubic, Pa-3, 205). *Materials Project* https://next-gen.materialsproject.org/materials/mp-20066#external_links.

- 55. Shin, Y. K., Gao, Y., Shin, D. & van Duin, A. C. T. Impact of three-body interactions in a ReaxFF force field for Ni and Cr transition metals and their alloys on the prediction of thermal and mechanical properties. *Comput. Mater. Sci.* **197**, 110602 (2021).
- 56. Birch, F. Finite Elastic Strain of Cubic Crystals. Phys. Rev. 71, 809–824 (1947).
- 57. Ravindran, P. *et al.* Density functional theory for calculation of elastic properties of orthorhombic crystals: Application to TiSi2. *J. Appl. Phys.* **84**, 4891–4904 (1998).
- 58. Tsuzuki, S., Uchimaru, T., Mikami, M. & Tanabe, K. Intermolecular interaction potential of the carbon dioxide dimer. *J. Chem. Phys.* **109**, 2169–2175 (1998).
- 59. Grimme, S. Accurate description of van der Waals complexes by density functional theory including empirical corrections. *J. Comput. Chem.* **25**, 1463–1473 (2004).
- 60. Klimeš, J., Bowler, D. R. & Michaelides, A. Van der Waals density functionals applied to solids. *Phys. Rev. B* **83**, 195131 (2011).
- 61. Kowalczyk, T. & Krylov, A. I. Electronic Structure of Carbon Trioxide and Vibronic Interactions Involving Jahn–Teller States. *J. Phys. Chem. A* **111**, 8271–8276 (2007).
- 62. Sabin, J. R. & Kim, H. A theoretical study of the structure and properties of carbon trioxide. *Chem. Phys. Lett.* **11**, 593–597 (1971).
- 63. DeMore, W. B. & Jacobsen, C. W. Formation of carbon trioxide in the photolysis of ozone in liquid carbon dioxide. *J. Phys. Chem.* **73**, 2935–2938 (1969).
- 64. J. Bennett, C., Jamieson, C., M. Mebel, A. & I. Kaiser, R. Untangling the formation of the cyclic carbon trioxide isomer in low temperature carbon dioxide ices. *Phys. Chem. Chem. Phys.* **6**, 735–746 (2004).

- 65. Jamieson, C. S., Mebel, A. M. & Kaiser, R. I. Identification of the D3h Isomer of Carbon Trioxide (CO3) and Its Implications for Atmospheric Chemistry. *ChemPhysChem* 7, 2508–2513 (2006).
- 66. Müller, C. & Usvyat, D. Incrementally Corrected Periodic Local MP2 Calculations: I. The Cohesive Energy of Molecular Crystals. *J. Chem. Theory Comput.* **9**, 5590–5598 (2013).
- 67. Cygan, R. T., Romanov, V. N. & Myshakin, E. M. Molecular Simulation of Carbon Dioxide Capture by Montmorillonite Using an Accurate and Flexible Force Field. *J. Phys. Chem. C* **116**, 13079–13091 (2012).
- 68. Chen, L., Wang, S. & Tao, W. A study on thermodynamic and transport properties of carbon dioxide using molecular dynamics simulation. *Energy* **179**, 1094–1102 (2019).
- 69. Muhunthan, P., Paredes Mellone, O., Kroll, T., Sokaras, D. & Ihme, M. The Local Electronic Structure of Supercritical CO2 from X-ray Raman Spectroscopy and Atomistic-Scale Modeling. *J. Phys. Chem. Lett.* **14**, 4955–4961 (2023).
- Liao, G., Du, Y., Zhang, F. & E, J. The Applications of Molecular Dynamics Simulation in Supercritical Carbon Dioxide: A Review. SSRN Scholarly Paper at https://doi.org/10.2139/ssrn.4097929 (2022).
- 71. Thermophysical Properties of Fluid Systems. https://webbook.nist.gov/chemistry/fluid/.
- 72. Cabral, B. J. C., Rivelino, R., Coutinho, K. & Canuto, S. A first principles approach to the electronic properties of liquid and supercritical CO2. *J. Chem. Phys.* **142**, 024504 (2015).
- 73. Gong, S., Wang, P. & Mo, Y. Bond Dissociation Energy of CO2 with Spectroscopic Accuracy Using State-to-State Resolved Threshold Fragment Yield Spectra. *J. Phys. Chem. Lett.* **15**, 10842–10848 (2024).